Article

Cell Reports

SENP3 Suppresses Osteoclastogenesis by De-conjugating SUMO2/3 from IRF8 in Bone Marrow-Derived Monocytes

Graphical Abstract

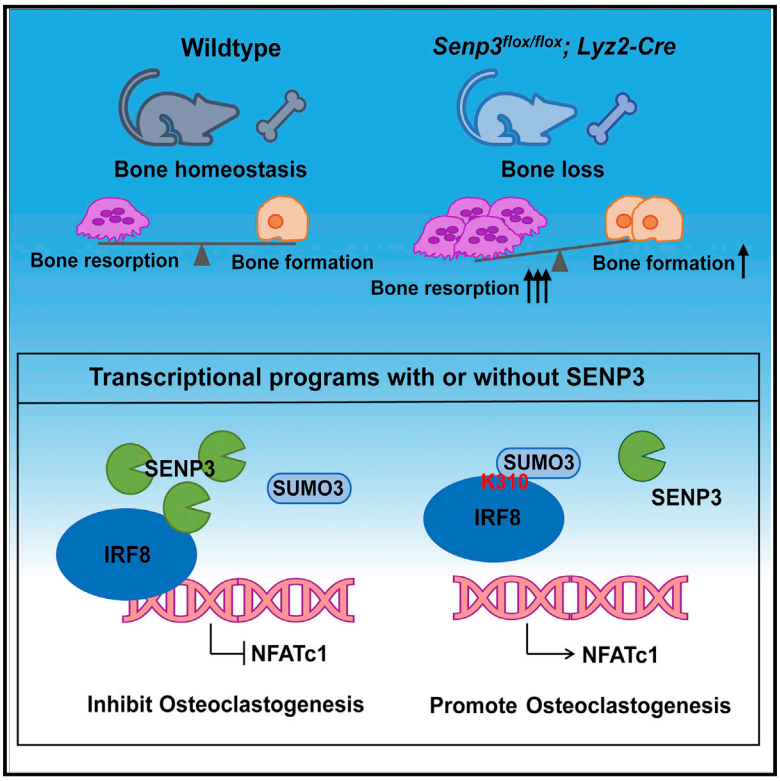

Highlights

- SENP3 decreases during osteoclastogenesis
- Loss of SENP3 in bone marrow-derived monocytes promotes osteoclast differentiation
- SENP3 suppresses osteoclast differentiation by de-conjugating SUMO2/3 from IRF8 at K310
- SENP3 overexpression partially protects against ovariectomy (OVX)-induced osteoporosis

Authors

Yongxing Zhang, Kai Yang, Jie Yang, ..., Jing Yi, Xuxu Sun, Qiugen Wang

Correspondence

yijing@shsmu.edu.cn (J.Y.), xuxu.sun@shsmu.edu.cn (X.S.), wangqiugen@126.com (Q.W.)

In Brief

Osteoclast over-activation leads to osteoporosis, but the role of post-translational modification in osteoporosis is not fully understood. Zhang et al. show that the SUMO protease SENP3 can alter the SUMO modification status on the critical osteoclast suppressor IRF8 in osteoclast precursor cells, which affects osteoclastogenesis and osteoporosis.

Zhang et al., 2020, Cell Reports *30*, 1951–1963
February 11, 2020
https://doi.org/10.1016/j.celrep.2020.01.036

CellPress

Cell Reports
Article

SENP3 Suppresses Osteoclastogenesis by De-conjugating SUMO2/3 from IRF8 in Bone Marrow-Derived Monocytes

Yongxing Zhang,[1,2,4] Kai Yang,[3,4] Jie Yang,[2] Yimin Lao,[2] Lianfu Deng,[3] Guoying Deng,[1] Jing Yi,[2,*] Xuxu Sun,[2,*] and Qiugen Wang[1,5,*]

[1]Trauma Center, Shanghai General Hospital, Shanghai Jiao Tong University School of Medicine, Shanghai 201620, China
[2]Shanghai Key Laboratory for Tumor Microenvironment and Inflammation, Department of Biochemistry and Molecular Cell Biology, Shanghai Jiao Tong University School of Medicine, Shanghai 200025, China
[3]Shanghai Key Laboratory for Prevention and Treatment of Bone and Joint Diseases with Integrated Chinese-Western Medicine, Shanghai Institute of Traumatology and Orthopedics, Ruijin Hospital, Shanghai Jiao Tong University School of Medicine, Shanghai 200025, China
[4]These authors contributed equally
[5]Lead Contact
*Correspondence: yijing@shsmu.edu.cn (J.Y.), xuxu.sun@shsmu.edu.cn (X.S.), wangqiugen@126.com (Q.W.)
https://doi.org/10.1016/j.celrep.2020.01.036

SUMMARY

Bone metabolism depends on the balance between osteoclast-driven bone resorption and osteoblast-mediated bone formation. Diseases like osteoporosis are characterized by increased bone destruction due to partially enhanced osteoclastogenesis. Here, we report that the post-translational SUMO modification is critical for regulating osteoclastogenesis. The expression of the SUMO-specific protease SENP3 is downregulated in osteoclast precursors during osteoclast differentiation. Mice with SENP3 deficiency in bone marrow-derived monocytes (BMDMs) exhibit more severe bone loss due to over-activation of osteoclasts after ovariectomy. Deleting SENP3 in BMDMs promotes osteoclast differentiation. Mechanistically, loss of SENP3 increases interferon regulatory factor 8 (IRF8) SUMO3 modification at the K310 amino acid site, which upregulates expression of the nuclear factor of activated T cell c1 (NFATc1) and osteoclastogenesis. In summary, IRF8 de-SUMO modification mediated by SENP3 suppresses osteoclast differentiation and suggests strategies to treat bone loss diseases.

INTRODUCTION

Osteoporosis is a common bone metabolic disease, characterized by systemic bone loss, disordered bone microstructure, and increased fragility (Schuit et al., 2004). Osteoporosis is divided into two major categories based on causes. Primary osteoporosis includes postmenopausal osteoporosis, senile osteoporosis, juvenile osteoporosis, and adult osteoporosis; secondary osteoporosis is mainly caused by long-term drug overuse (e.g., long-term use of glucocorticoid) (Di Iorgi et al., 2008). Among them, postmenopausal osteoporosis (also regarded as "estrogen-deficient osteoporosis") is the most common primary osteoporosis disease (Black and Rosen, 2016).

Bone homeostasis requires a delicate balance between osteoblast-mediated bone formation and osteoclast-mediated bone resorption. Although estrogen deficiency occurring after menopause activates both osteoblasts and osteoclasts, activation of the latter dominates and quickly leads to decreased bone mass. Therefore, preventing osteoclast activation is one way to treat postmenopausal osteoporosis patients in clinics. Indeed, various osteoclast inhibitors were reported to reduce bone loss and prevent fragility fractures (Black et al., 1996; Cummings et al., 2009; Ettinger et al., 1999; Harris et al., 1999; Matsumoto et al., 2009). However, these inhibitors also caused side effects, such as increased risks of endometrial lesions (Black and Rosen, 2016), suggesting an ongoing need for new therapeutic strategies and clarifications of detailed mechanisms underlying osteoclast activation.

Osteoclasts are multi-nucleated cells formed by the fusion of osteoclast precursor cells from bone marrow-derived monocytes (BMDMs). Osteoclast differentiation requires two cytokines: macrophage colony stimulating factor (M-CSF) and receptor activator of nuclear factor κB (NF-κB) ligand (RANKL). M-CSF maintains survival and proliferation of osteoclast precursor cells. The ligand RANKL binds to the receptor RANK on BMDMs, leading to the recruitment of tumor necrosis factor (TNF) receptor-associated factor 6 (TRAF6) on the target gene promotors, subsequently activating downstream c-Jun N-terminal kinase (JNK), p38, or extracellular signal-regulated kinase (ERK) signaling pathways (Takayanagi et al., 2002, 2007; Teitelbaum, 2000) to induce BMDMs to proliferate and differentiate into osteoclasts. In addition, RANKL activates other critical transcription factors, such as NF-κB, microphthalmia-associated transcription factor (MITF), c-*fos*, and nuclear factor-activated T cell c1 (NFATc1), to promote the fusion of osteoclast precursor cells and osteoclast maturation.

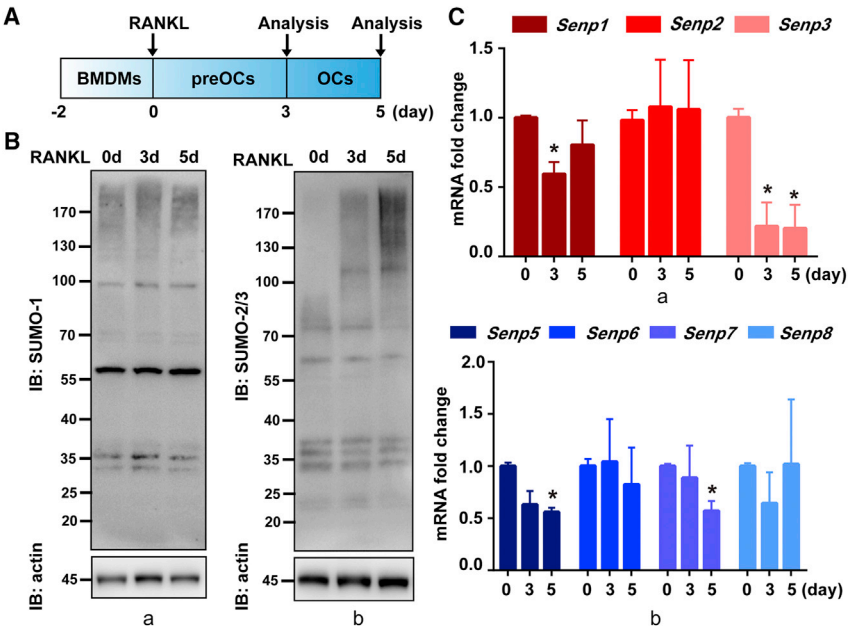

Figure 1. SUMO2/3 Modification Increased and the Expression of SENP3 Decreased during Osteoclastogenesis

(A) Schema for BMDM differentiation stages *in vitro*. BMDMs were cultured with M-CSF and RANKL. Analysis was conducted during proliferation (BMDMs), differentiation (osteoclast precursors [preOCs]), and maturation (osteoclasts [OCs]) stages at indicated days (arrow).

(B) SUMO-1 (a) and SUMO2/3 (b) modification in BMDMs at different days after RANKL induction, as measured by western blot with SUMO1 and SUMO2/3 antibodies.

(C) SENP family mRNA expression in BMDMs at different days after RANKL induction, as measured by qPCR.

All data in this figure are represented as mean ± SD. *$p < 0.05$. All experiments were performed in triplicates.

See also Figure S1 and Table S1 for qPCR primer sequences.

NFATc1 is a key transcription factor for osteoclast differentiation and, together with MITF and c-*fos*, regulates osteoclast-specific genes, such as TRAP, cathespsin K (CTSK), calcitonin receptor (CTR), and osteoclast-associated receptor (OSCAR) (Kim et al., 2005a, 2005b; Matsumoto et al., 2004; Takayanagi et al., 2002). Studies showed that overexpressing *NFATc1* in osteoclast precursor cells could induce osteoclast maturation even in the absence of RANKL, indicating that NFATc1 is an indispensable factor for osteoclast differentiation. To date, many genes were discovered to inhibit NFATc1 function, such as RANKL attenuates differentiation inhibitors (Ids), V-maf muscle decidual fibrosarcoma oncogene homolog B (MafB), activated STAT3 protein inhibitor (PIAS3), LIM homeobox gene 2 (Lhx2), Bcl-6, and interferon regulatory factor-8 (IRF-8), that could downregulate *NFATc1* expression that negatively regulates osteoclastogenesis (Kim et al., 2007a, 2007b, 2014; Lee et al., 2006; Miyauchi et al., 2010; Zhao et al., 2009). Deletion of *Lhx2*, *IRF-8*, and *Bcl-6* genes in mice resulted in severe osteoporosis (Kim et al., 2014; Miyauchi et al., 2010; Zhao et al., 2009). Therefore, negatively regulating NFATc1 during osteoclastogenesis will be a potential therapeutic strategy.

SUMO modification is a reversible post-translational protein modification that is used in a wide spectrum of cellular processes. Similar to ubiquitination, SUMOylation occurs when proteins are modified with the small-molecule proteins SUMO1, SUMO2, or SUMO3 after a series of catalytic reactions by E1, E2, and E3 enzymes. The modified substrates can be de-conjugated by a SUMO-specific protease from the SUMO-specific protease (SENP) family, in a process called de-SUMOylation. Seven SENPs (SENP1, 2, 3, 5, 6, 7, and 8) have been reported in mammals. Dynamics of SUMO and de-SUMO modifications result in the alteration of protein activity, localization, and protein-protein or protein-DNA interaction, consequently regulating cellular behavior (Wang and Dasso, 2009). Recent studies showed SUMOylation and SENPs have an impact on bone metabolism. SENP3 promoted osteogenesis by de-SUMOylating RbBP5, which activated the expression of *HOX* genes (Nayak et al., 2014). SENP6 de-SUMOylated and stabilized TRIM28, which suppressed p53 activity and then prevented skeletal senescence (Li et al., 2018). In addition, studies discovered that SUMOylation of specific inflammatory factors in BMDMs could inhibit the progress of inflammation and de-SUMOylation by SENPs promoted the activation of BMDMs to macrophage (Ghisletti et al., 2007; Huang et al., 2011; Pascual et al., 2005), However, there was little evidence for the association between SUMOylation and osteoclast differentiation. Here, we demonstrated that global SUMO2/3 modification increased, whereas the expression of SENP3 was decreased during osteoclastogenesis. Deleting the *Senp3* gene potentiated osteoclast differentiation and bone loss. Our study implies that SUMOylation is involved in the process of osteoclastogenesis and SENP3 has therapeutic potential as an osteoclast suppressor.

RESULTS

SUMO2/3 Modification Increased and the Expression of *Senp3* Decreased during Osteoclastogenesis

To assess if SUMO modification has a role in the process of osteoclast differentiation, we isolated primary osteoclast progenitors (i.e., BMDMs) from C57BL/6 mice and induced osteoclast differentiation *in vitro* by M-CSF and RANKL (Figure 1A). During osteoclastogenesis, SUMO1 modification remained stable, whereas SUMO2/3 modification increased over time (Figure 1B). Because SUMOylation is reversibly regulated by SUMO ligases and a family of SUMO-specific proteases (SENPs), we then measured the expression of proteins/enzymes related to SUMO conjugation and de-conjugation by

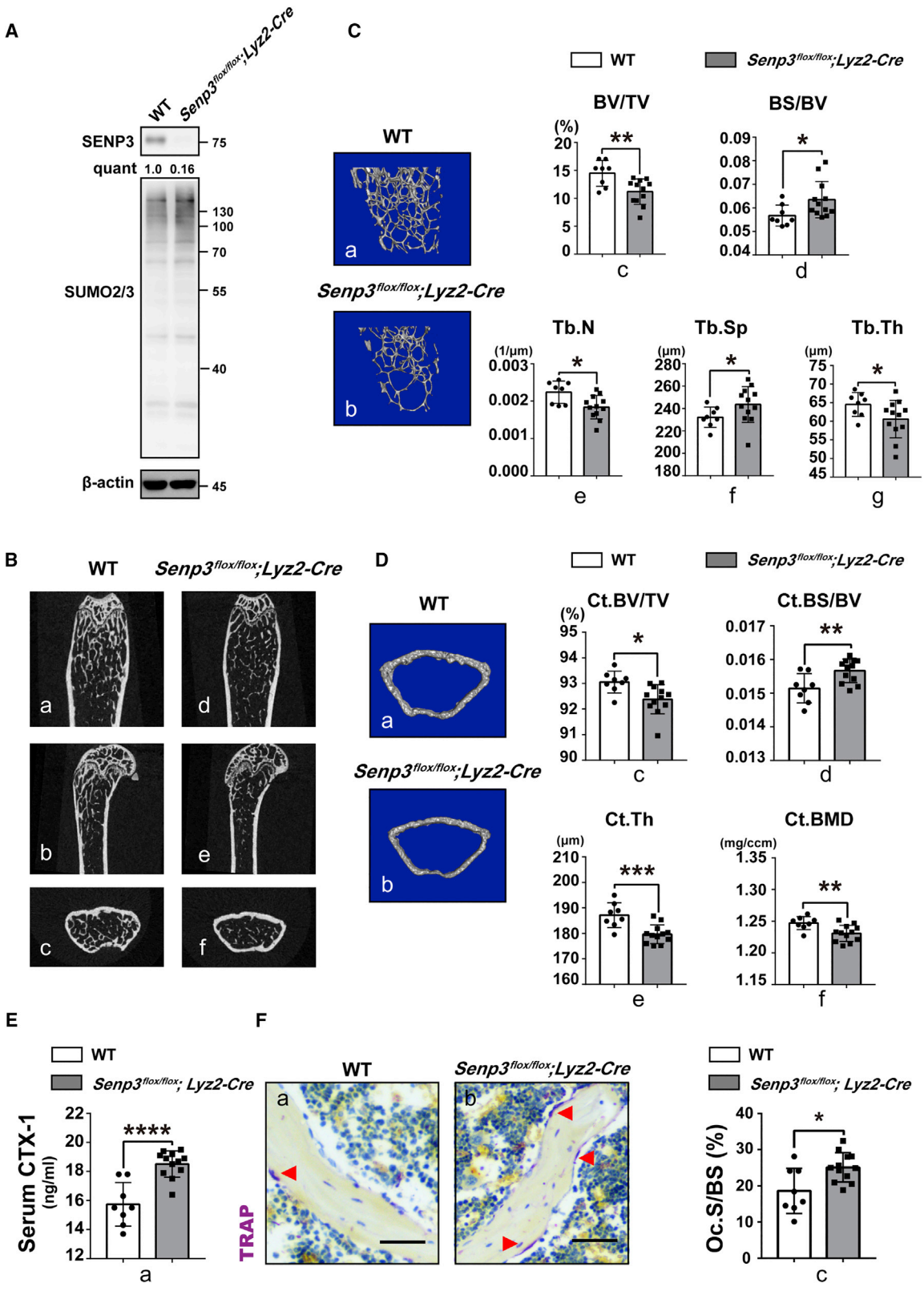

(legend on next page)

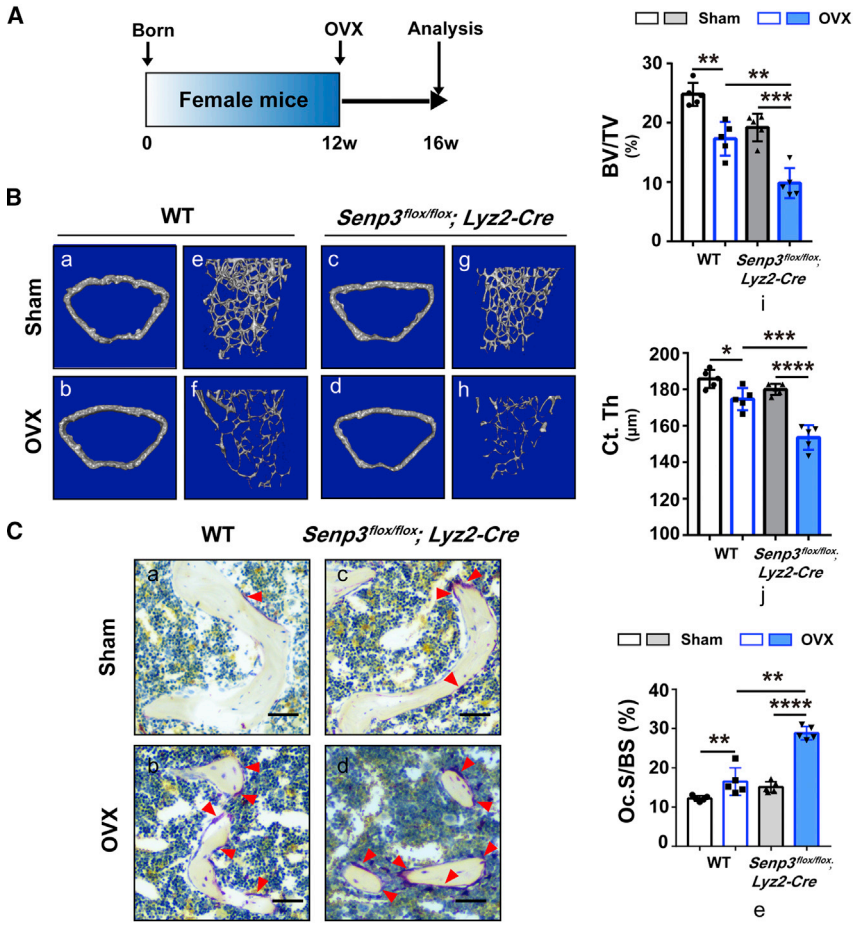

Figure 3. *Senp3*$^{flox/flox}$*; Lyz2-Cre* Mice Suffered More Severe Bone Loss in OVX Model

(A) Ovariectomy (OVX) was conducted in 12-week-old female WT and *Senp3*$^{flox/flox}$*; Lyz2-Cre* mice. Mice were collected for micro-CT and histological analysis 4 weeks later.

(B) 3D restoration of cortical (a, b, c, and d) and cancellous (e, f, g, and h), trabecular BV/TV (i), and cortical thickness (Ct.Th) (j) after OVX or sham, as measured by micro-CT scan (n = 5, WT; and n = 5, *Senp3*$^{flox/flox}$*; Lyz2-Cre*).

(C) TRAP staining on paraffin-embedded bone sections in WT (a and b) and *Senp3*$^{flox/flox}$*; Lyz2-Cre* (c and d) mice after OVX/sham experiment (scale bar, 100 μm; red arrowheads point to TRAP positive osteoclasts); osteoclast surface/bone surface ratios (Oc.S/BS) (e) are shown on the right.

All data in this figure are represented as mean ± SD. *p < 0.05, **p < 0.01, ***p < 0.005, ****p < 0.001. All experiments were performed in triplicates.

Senp3$^{flox/flox}$*; Lyz2-Cre* Mice Have Less Bone Mass with More Active Bone Resorption

To further determine whether the loss of SENP3 promotes osteoclastogenesis, we generated BMDM-specific *Senp3* knockout mice (*Senp3*$^{flox/flox}$*; Lyz2-Cre*) by using Cre driven by *Lyz2* (*Lysosome C-2*) promoters (Bae et al., 2017; Lao et al., 2018). *Senp3* was specifically knocked out in BMDMs, and there was little difference in the expression of *SUMO1*, *SUMO2*, *SUMO3*, *SAE1*, *SAE2*, and *Ubc9* between *Senp3*$^{flox/flox}$ (referred to as wild type [WT] hereafter) and *Senp3*$^{flox/flox}$*; Lyz2-Cre* BMDMs (Figures 2A and S2).

qPCR. During osteoclast differentiation, the expression of *SUMO1*, *SUMO2*, *SUMO3*, *SAE1* (E1 enzyme), *SAE2* (*UBA2*, E1 enzyme), and *Ubc9* (E2 enzyme) was nearly unchanged (Figure S1), whereas the expression of *Senp3* and *Senp5* was dramatically decreased (Figure 1C). Altogether, these data suggested that post-translational SUMO2/3 modification is enhanced in the process of osteoclastogenesis, which might be associated with reduced *Senp3* or *Senp5* expression.

In micro-computed tomography (CT) analysis, *Senp3*$^{flox/flox}$*; Lyz2-Cre* mice showed less bone mass in the distal femur (Figure 2B) with significantly reduced trabecular bone mass (Figures 2Ca and 2Cb), shown by decreased bone volume/tissue volume ratio (BV/TV), trabecular number (Tb.N), and trabecular thickness (Tb.Th) and increased bone surface/bone volume

Figure 2. *Senp3*$^{flox/flox}$*; Lyz2-Cre* Mice Had Less Bone Mass with More Active Bone Resorption

(A) SENP3 expression and SUMO2/3 modification in 12-week-old *Senp3*$^{flox/flox}$ (referred to as WT) and *Senp3*$^{flox/flox}$*; Lyz2-Cre* BMDMs, as measured by western blot.

(B) Represented images of the coronal (a and d), sagittal (b and e), and transverse (c and f) of distal femur in 12-week-old mice, as measured by micro-CT 2D restoration (n = 8, WT; and n =12, *Senp3*$^{flox/flox}$*; Lyz2-Cre*).

(C) Represented images of three-dimensional (3D) restoration (a and b), bone volume/tissue volume ratios (%) (BV/TV) (c), bone surface/bone volume (BS/BV) (d), trabecular number (Tb.N) (e), trabecular separation (Tb.Sp) (f), and trabecular thickness (Tb.Th) (g) of the distal femur cancellous bone in 12-week-old mice, as measured by micro-CT scan (n = 8, WT; and n =12, *Senp3*$^{flox/flox}$*; Lyz2-Cre*).

(D) Represented images of 3D restoration (a and b), bone volume/tissue volume ratios (%) (Ct.BV/TV) (c), bone surface/bone volume (Ct.BS/BV) (d), cortical thickness (Ct.Th) (e), and cortical bone mineral density (Ct.BMD) of the distal femur cortical bone in 12-week-old mice, as measured by micro-CT scan (n = 8, WT; and n =12, *Senp3*$^{flox/flox}$*; Lyz2-Cre*).

(E) Serum CTX-1 was detected by ELISA (n = 8, WT; and n =12, *Senp3*$^{flox/flox}$*; Lyz2-Cre*).

(F) TRAP staining of distal femur on paraffin-embedded bone sections in WT (a) and *Senp3*$^{flox/flox}$*; Lyz2-Cre* (b) mice (scale bar, 100 μm; red arrow heads point to TRAP-positive osteoclasts); osteoclast surface/bone surface ratios (Oc.S/BS) (c) are shown on the right.

All data in this figure are represented as mean ± SD. *p < 0.05, **p < 0.01, ***p < 0.005, ****p < 0.001. All experiments were performed in triplicates.

See also Figures S2 and S3.

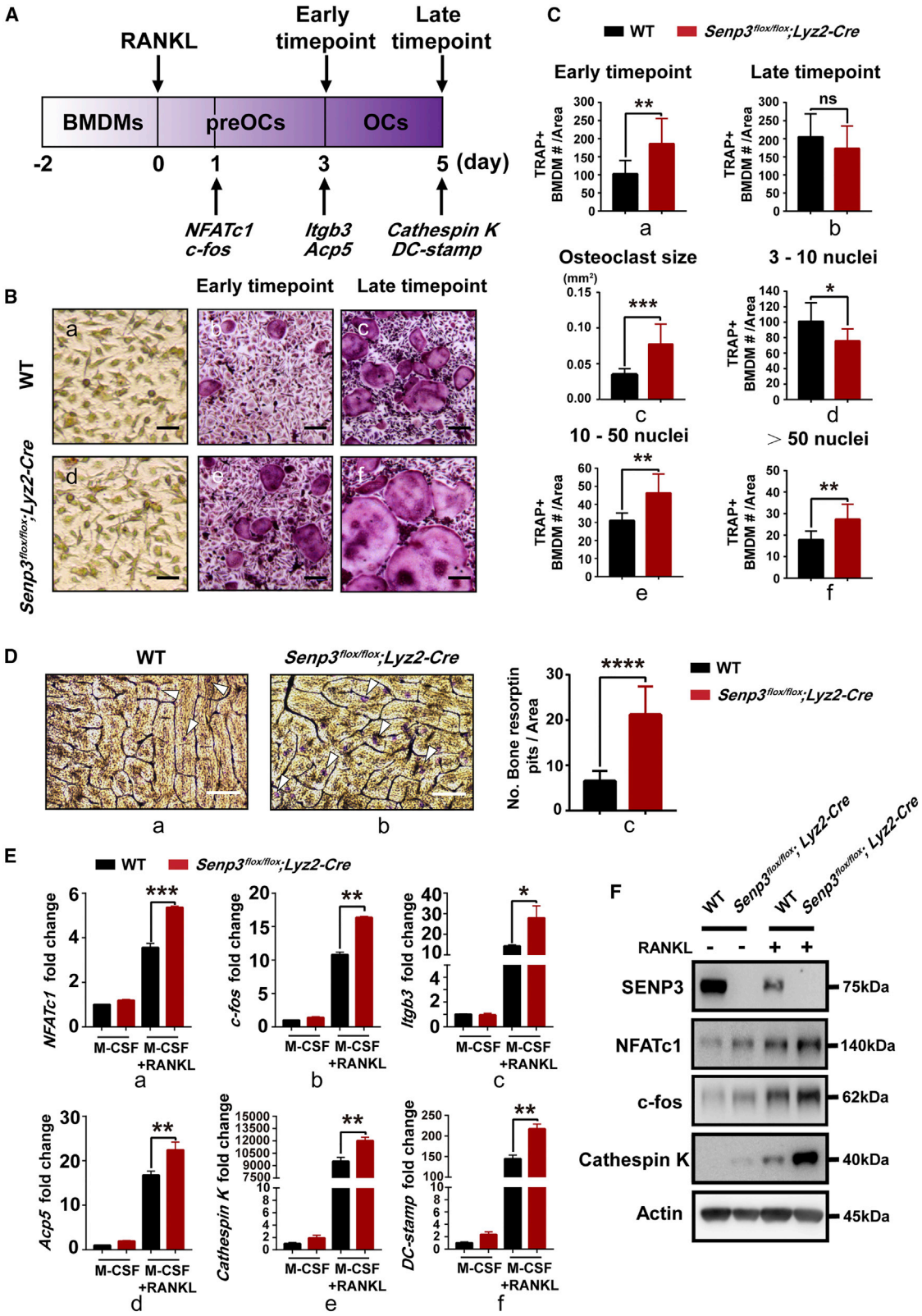

(legend on next page)

ratio (BS/BV) and trabecular separation (Tb.Sp) (Figures 2Cc–2Cg). There was also thinner cortical bone (Figures 2Da and 2Db) in *Senp3*$^{flox/flox}$*; Lyz2-Cre* mice, as shown by decreased bone volume/tissue volume ratio (Ct.BV/TV), bone mineral density (Ct.BMD), and cortical thickness (Ct.Th) and increased bone surface/bone volume ratio (Ct.BS/BV) (Figures 2Dc–2Df). We then assessed the mineral apposition rate (MAR) and bone formation rate/bone surface ratio (BFR/BS) by calcien staining, and the results showed that *Senp3*$^{flox/flox}$*; Lyz2-Cre* mice had a significantly improved bone remodeling rate (Figure S3A). These data demonstrate that *Senp3*$^{flox/flox}$*; Lyz2-Cre* mice exhibit modest bone loss compared to the WT littermates and genetic deletion of *Senp3* in BMDMs accelerated the baseline bone turnover rate.

To examine if SENP3 loss in BMDMs disrupted the dynamic balance between osteoclasts and osteoblasts, we measured the markers for bone resorption and bone formation. *Senp3*$^{flox/flox}$*; Lyz2-Cre* mice had a greater value of serum C-terminal telopeptide for type 1 collagen (CTX-1), suggesting enhanced bone resorption and osteoclast activity (Figure 2E). In addition, more TRAP-positive osteoclasts shown by TRAP staining (Figure 2F) were found on the surface of trabecular bone in *Senp3*$^{flox/flox}$*; Lyz2-Cre* mice, which is consistent with the CTX-1 serological evidence. However, there was also a greater number of osteoblasts and an increased level of procollagen type 1 N-propeptide (P1NP) in *Senp3*$^{flox/flox}$*; Lyz2-Cre* mice (Figures S3B and S3C), which suggest enhanced bone formation and osteoblast activity as well.

To determine if the enhanced bone formation is due to the increased bone resorption, we isolated bone marrow stromal cells (BM-MSCs) from WT and *Senp3*$^{flox/flox}$*; Lyz2-Cre* mice and induced osteogenic differentiation *in vitro*. After induction, alkaline phosphatase (ALP) staining and alizarin red staining after the induction showed that there was no difference in the potential of osteogenic differentiation in BM-MSCs from the two genotypes of mice (Figure S3D). Consistently, the expression of osteogenesis-specific genes *Runx2*, *Ostrix*, *OCN*, and *Atf4* was not changed between BM-MSCs from WT and *Senp3*$^{flox/flox}$*; Lyz2-Cre* mice (Figure S3E). Normal *in vitro* differentiation and activity of osteoblasts from *Senp3*$^{flox/flox}$*; Lyz2-Cre* mice suggest the improved osteoclast function in *Senp3*$^{flox/flox}$*; Lyz2-Cre* mice resulted in enhanced osteoblast activity *in vivo*.

Altogether, these data showed that *Senp3* loss in BMDMs contributed to the enhanced bone turnover and remodeling due to accelerated bone resorption accompanied by mildly increased bone formation, eventually resulting in excessive bone mass loss.

Senp3$^{flox/flox}$*; Lyz2-Cre* Mice Suffered More Severe Bone Loss in the OVX Model

To further investigate the function of SENP3 in osteoclastogenesis, we performed ovariectomy (OVX), which is a classic model mimicking postmenopausal osteoporosis (Figure 3A) (Kanis et al., 2013). Four weeks after OVX, *Senp3*$^{flox/flox}$*; Lyz2-Cre* mice exhibited more severe osteoporosis, as shown by reduced bone mass in the distal femur, a lower level of cancellous BV/TV, and thinner Ct.Th (Figures 3Ba–3Bj). The TRAP staining on the paraffin-embedded bone sections showed more TRAP-positive osteoclasts adhering to the surface of the trabecular bone (Figures 3Ca–3Ce) in *Senp3*$^{flox/flox}$*; Lyz2-Cre* mice. These data demonstrated that after estrogen deprivation, the loss of SENP3 resulted in more severe osteoporosis that might be due to the enhanced capability of osteoclastogenesis.

SENP3 Loss in BMDMs Accelerated Osteoclastogenesis

To test the effect of SENP3 loss on osteoclast differentiation, we isolated BMDMs from WT and *Senp3*$^{flox/flox}$*; Lyz2-Cre* mice. M-CSF and RANKL were administered to induce BMDM differentiation into osteoclasts (Figure 4A). At different time points, we collected differentiated BMDMs for TRAP staining (Figure 4B). The results showed a greater number of TRAP-positive cells from BMDMs in *Senp3*$^{flox/flox}$*; Lyz2-Cre* mice than that in WT littermates after RANKL induction at an early time point (Figures 4Ca and 4Cb). The TRAP-positive osteoclast size was larger (Figure 4Cc) and the numbers of nuclei per cell were significantly higher in BMDMs from *Senp3*$^{flox/flox}$*; Lyz2-Cre* mice (Figures 4Cd–4Cf). To assess the function of osteoclasts, we analyzed the number of bone resorption pits on bone slices by using the bone resorption assay. The results showed that osteoclasts differentiated from BMDMs from *Senp3*$^{flox/flox}$*; Lyz2-Cre* mice had a stronger ability for bone absorption (Figure 4D). We then further examined the expression of osteoclast-specific genes in BMDMs from WT and *SENP3*$^{flox/flox}$*; Lyz2-Cre* mice before and after RANKL induction by qPCR and western blot. *NFATc1*, *c-fos*, *Itgb3*, *Acp5*, *Cathespin K*, and *DC-stamp* were elevated after RANKL induction, especially in BMDMs from *SENP3*$^{flox/flox}$*; Lyz2-Cre* mice (Figure 4E). Consistently, NFATc1, c-*fos*, and Cathespin K were increased also at the protein level (Figure 4F). In sum, SENP3 loss promoted BMDM differentiation and osteoclastogenesis.

Figure 4. SENP3 Loss in BMDMs Accelerated Osteoclastogenesis

(A) BMDMs from WT and *Senp3*$^{flox/flox}$*; Lyz2-Cre* mice were collected and induced differentiation with M-CSF and RANKL treatment. Different osteoclast-specific genes were analyzed at proliferation (BMDMs), differentiation (preOCs), and maturation (OCs) stages.

(B) TRAP staining of BMDMs (a and d), preOCs (early time point) (b and e), and OCs (late time point) (c and f) (scale bar, 100 μm).

(C) Number of TRAP+ BMDMs in one field of vision at early time point (a) and late time point (b); osteoclast size of TRAP+ BMDMs (c); and the number of TRAP+ BMDMs with 3–10 nuclei (d), 10–50 nuclei (e), and >50 nuclei (f) were measured respectively.

(D) Bone resorption assay was conducted on bovine cortical bone slices in 48-well plates with BMDMs from WT and *Senp3*$^{flox/flox}$*; Lyz2-Cre* mice. Bone resorption pits were measured by toluidine blue staining 7 days after M-CSF/RANKL treatment (a and b) (scale bar, 1 mm; white arrowheads point to osteoclast-mediated bone resorption pits); quantification of bone resorption pit numbers is shown on the right (c).

(E) *NFATc1* (a), *c-fos* (b), *Itgb3* (c), *Acp5* (d), *Cathespin K* (e), and *DC-stamp* (f) mRNA levels in BMDMs, as measured by qPCR.

(F) SENP3, NFATc1, c-*fos*, and Cathespin K protein levels in BMDMs, as measured by western blot.

All data in this figure are represented as mean ± SD. *p < 0.05, **p < 0.01, ***p < 0.005, ****p < 0.001. All experiments were performed in triplicates.

See also Table S1 for qPCR primer sequences

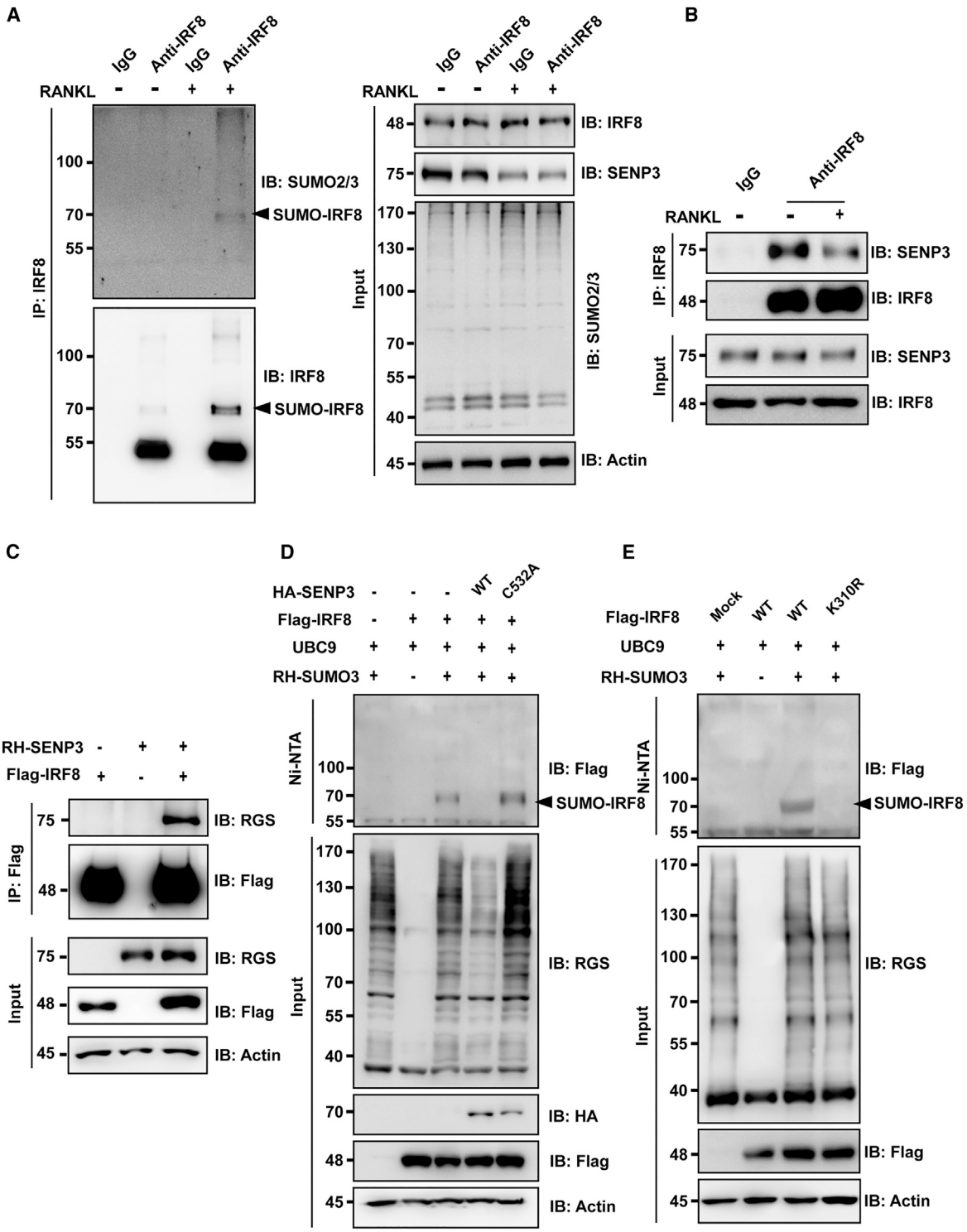

Figure 5. The SUMOylation of IRF8 Increased during Osteoclast Differentiation, and SENP3 Catalyzes De-SUMOylation of IRF8 at the Site K310

(A) The endogenous SUMOylation of IRF8 in BMDMs. BMDMs were collected before and after treatement with RANKL for 3 days, and whole-cell lysates were used for pull-down assay. IP was performed with IRF8 antibody, and immunoblotting (IB) was performed with SUMO2/3, SENP3, and IRF8 antibodies.

(B) The endogenous SENP3 and IRF8 interaction in BMDMs before and after treatement with RANKL for 3 days, as measured by coIP. Pull-down assay was performed with IRF8 antibody, and IB was performed with SENP3 and IRF8 antibodies

(legend continued on next page)

SENP3 Catalyzes De-SUMOylation of IRF8 at the K310 Site

To investigate the molecular mechanisms underlying the promotion of osteoclastogenesis in *Senp3*-deficient mice, we focused on identifying SENP3 substrates in BMDMs. Our previous studies discovered that SUMO2/3 modification of specific kinase or transcriptional factors inhibited their activity (Huang et al., 2009; Lao et al., 2018), which was reversed by SENP3-mediated de-SUMOylation. We hypothesized that SENP3 loss may alter the activity of key osteoclast-differentiation-related transcriptional factors by de-conjugating SUMO2/3. Based on the protein SUMOylation prediction system (Hendriks et al., 2018), we tested the potential SUMO2/3 modification of transcriptional factors related to osteoclastogenesis *in vitro*. None of these transcriptional factors could be modified by SUMO2/3 in our system (data not shown). We then used a SUMO prediction software (http://www.jassa.fr/) to screen all the other factors related to osteoclast differentiation and found interferon regulatory factor 8 (IRF8), a critical suppressor of the critical transcriptional factor NFATc1, to have a high score of SUMO modification. To validate SUMO2/3 modification of IRF8 during osteoclastogenesis, we performed a co-immunoprecipitation (coIP) assay using primary BMDMs derived from WT mice. The result showed that after RANKL induction, IRF8 was dramatically modified by SUMO2/3 (Figure 5A), whereas the interaction of SENP3 and IRF8 was diminished (Figure 5B). In addition, SUMO2/3-conjugated IRF8 displayed a prominent band on the gel at 70 kDa molecular weight, indicating a single SUMO protein conjugation.

To further study de-SUMOylation of IRF8 by SENP3, we utilized the HEK293T overexpression system. By overexpressing FLAG-IRF8 and RH-SENP3, we confirmed the SENP3 interaction with IRF8 (Figure 5C). We then overexpressed SENP3 WT and SENP3 C532A mutant, which lacks SENP3 de-SUMOylation activity. SENP3 WT overexpression was sufficient to de-conjugate SUMO3 from IRF8 in cells, whereas the SENP3 mutant was not (Figure 5D). Additionally, we used the knockdown system to further assess if the de-SUMOylation of IRF8 required SENP3. We transfected scramble-small interfering RNA (siRNA) or SENP3-siRNA in HEK293T cells and found that SENP3 knockdown increased SUMO3 modification on IRF8 (Figure S4).

Next, we identified the specific amino acid residues that were modified by SUMO3 on IRF8 by constructing an IRF8 plasmid with a Lysine-310-to-Arginine mutation according to the SUMO prediction software (http://www.jassa.fr/) and the report from Chang et al. (2012). The SUMOylation assay demonstrated that SUMO3 modification on IRF8 was abolished when K310 was mutated to R (Figure 5E). By knocking down SENP3, we further confirmed that the IRF8 K310R mutant could not be conjugated with SUMO3 (Figure S4). These data verified IRF8 as the substrate of SENP3, and K310 was the site for SUMO3 modification. Altogether, we found that SUMOylation of IRF8 increased during osteoclastogenesis, which was due to the diminished interaction with SENP3. The Lysine 310 of IRF8 was the site for SUMO3 conjugation, and SUMOylation of IRF8 may contribute to osteoclastogenesis.

Loss of SUMO3 Modification of IRF8 Was Sufficient to Suppress NFATc1 Expression and Abolished Osteoclastogenesis

NFATc1 is the key transcription factor to promote osteoclastogenesis, and its expression is negatively regulated by IRF8. To test whether SENP3 loss mediated by IRF8 SUMOylation at the K310 site contributes to NFATc1 expression and osteoclastogenesis, we overexpressed IRF8 WT and IRF8 K310R mutant in primary BMDMs with scramble-siRNA or SENP3-siRNA and then induced osteoclast differentiation by RANKL (Figure 6A). We found that RANKL induction and SENP3 knockdown did not affect IRF8 WT and mutant expression levels, as shown by consistent FLAG-tagged proteins (Figure 6B). NFATc1 expression was downregulated in cells overexpressing IRF8 K310R compared to IRF8 WT, which suggests that the loss of SUMOylation at IRF8 K310R further inhibited NFATc1 expression during osteoclastogenesis (Figure 6B). Correspondingly, the IRF8 K310R BMDMs showed reduced numbers and sizes of TRAP-positive osteoclasts after RANKL induction (Figure 6C). We then compared the effect of scramble- and SENP3-siRNAs during osteoclastogenesis. Knocking down SENP3 increased NFATc1 expression and the number of TRAP-positive BMDMs when cells overexpressed IRF8 WT but not IRF8 K310R (Figures 6B and 6C). Consistently, the osteoclast differentiation markers *Itgb3*, *Cathespin K*, *Acp5*, *DC-Stamp*, and *Atp6v0d2* were all increased after knocking down SENP3 in IRF8 WT cells but not in IRF8 K310R cells (Figure 6D). Altogether, these data demonstrate that SENP3 deficiency promoted osteoclastogenesis, which required IRF8 K310 SUMO modification. The loss of IRF8 SUMOylation is sufficient to suppress NFATc1 expression and osteoclastogenesis.

Overexpressing SENP3 Rescued Osteoclast Differentiation

Next, we overexpressed SENP3 to test the anti-osteoporosis effect. We isolated BMDMs and overexpressed SENP3 WT or SENP3 C532A mutant plasmids. After M-CSF and RANKL

(C) The exogenous interaction of SENP3 with IRF8 was determined by coIP. HEK293T cells were transfected with RH-SENP3 and FLAG-IRF8 plasmids for 48 h. IP was performed using FLAG-M2 beads; FLAG and RGS antibodies were used for IB.
(D) SUMO3 conjugates to IRF8 were determined by Ni-bead pull down. FLAG-IRF8, RH-SUMO3, and UBC9 were co-transfected into HEK293T cells along with HA-SENP3 or HA-SENP3 C532A mutant for 48 h. RH-SUMO3 was pulled down using Ni-NTA beads and then analyzed by IB as indicated.
(E) HEK293T cells were co-transfected with FLAG-IRF8 WT or mutated FLAG-IRF8 K310R, RH-SUMO3, and UBC9 as indicated for 48 h. Cells were lysed, and RH-SUMO3 was pulled down using Ni-NTA beads and then analyzed by IB as indicated.
Arrowheads indicated SUMO3-conjugated IRF8 (B, D, and E).
See also Figure S4.

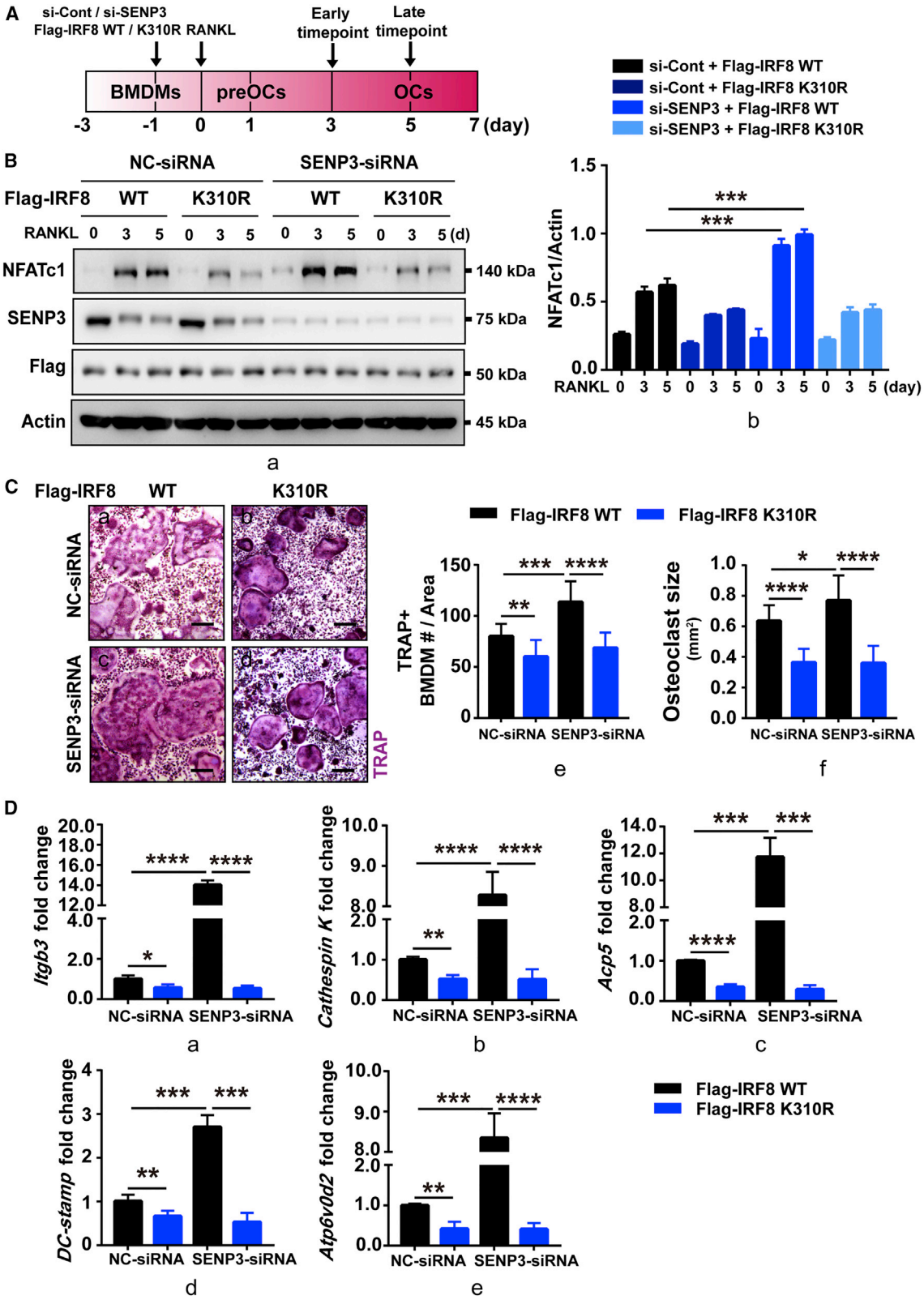

(legend on next page)

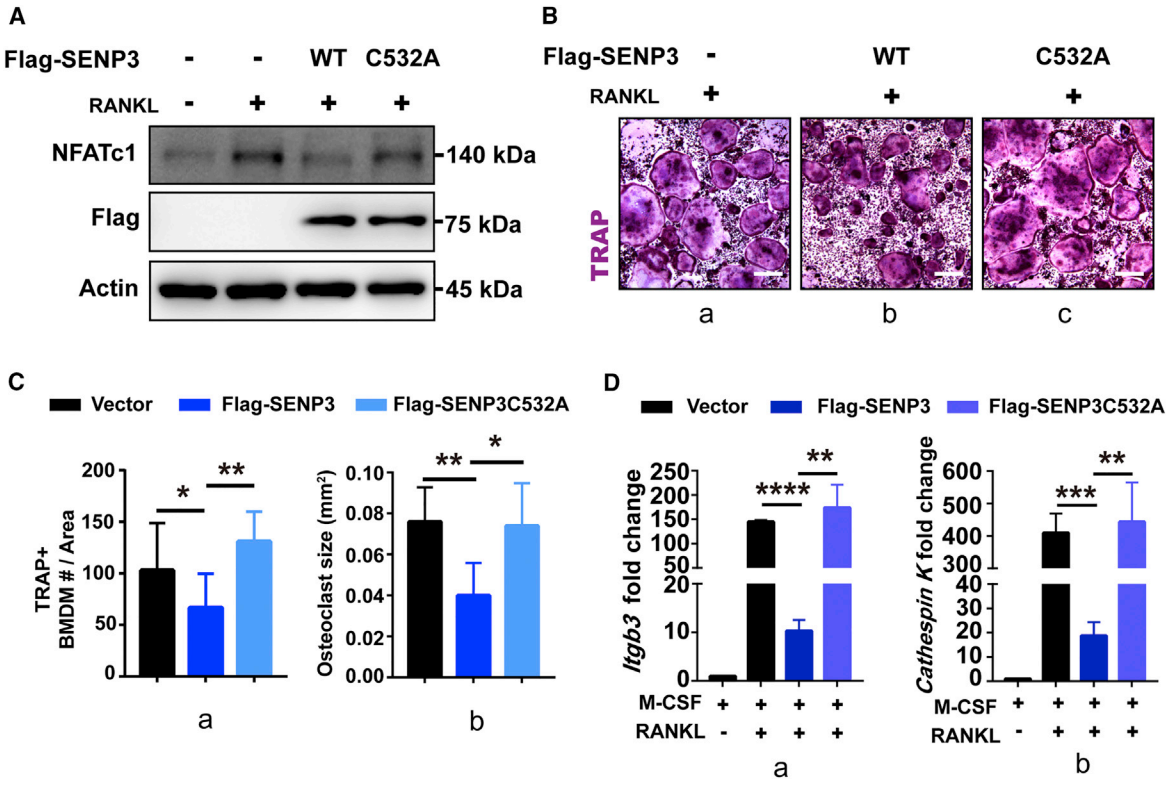

Figure 7. Overexpressing SENP3 Rescued Osteoclast Differentiation

(A) BMDMs transfected with FLAG-SENP3 WT and FLAG-SENP3 C532A mutant for 48 h and then incubated with M-CSF and RANKL for 3 days. NFATc1 expression was measured by western blot.

(B) BMDMs transfected with FLAG-Vector(a), FLAG-SENP3 WT (b), and FLAG-SENP3 C532A (c) for 48 h and then incubated with M-CSF and RANKL for 5 days. Histology of BMDMs were measured by TRAP staining (scale bar, 100 μm).

(C) Quantification of TRAP-positive BMDM numbers in one field (a) and TRAP-positive BMDM size (b) were analyzed.

(D) BMDMs transfected with FLAG-SENP3 WT and FLAG-SENP3 C532A mutant for 48 h and then incubated with M-CSF and RANKL for 5 days. The expression of *Itgb3* (a) and *Cathespin K* (b) were measured by qPCR.

All data in this figure are represented as mean ± SD. *p < 0.05, **p < 0.01, ***p < 0.005, ****p < 0.001. All experiments were performed in triplicates.

See also Table S1 for qPCR primer sequences.

induction, the expression of NFATc1 was suppressed with SENP3 WT cells but not in SENP3 C532A mutant cells (Figure 7A). TRAP staining showed that there were more and larger TRAP-positive BMDMs with SENP3 C532A mutant overexpression than with SENP3 WT overexpression (Figures 7B and 7C). The qPCR analysis also confirmed that osteoclast-specific genes decreased in SENP3 overexpressing cells compared to SENP3 C532A mutant cells (Figure 7D). These results together revealed that SENP3-overexpression-mediated de-SUMOylation could reduce osteoclastogenesis and, thus, suggested that SENP3 would be a critical factor to protect bone against osteoporosis.

DISCUSSION

Osteoporosis is a common chronic disease during aging and is especially common for postmenopausal women. Although osteoclast-inhibiting agents are used in the clinic, the

Figure 6. Loss of SUMO3 Modification of IRF8 Is Sufficient to Suppress NFATc1 Expression and Abolish Osteoclastogenesis

(A) Schema of BMDM treatment with siRNA. Scramble-siRNA and SENP3-siRNA were co-transfected with FLAG-IRF8 WT or FLAG-IRF8 K310R into BMDMs, respectively. BMDMs were analyzed at indicated days after M-CSF and RANKL treatment.

(B) The expression of NFATc1, as measured by western blot and quantified by NFATc1/Actin ratio on the right.

(C) Histology of BMDMs at day 5 after siRNA$^+$ plasmid transfection and RANKL treatment, as measured by TRAP staining (late time point) (a–d). Quantification of TRAP-positive BMDM number in one field of vision (early time point) (e), and TRAP-positive BMDM sizes (late time point) (f) were shown as indicated (scale bar, 100 μm).

(D) *Itgb3* (a), *Cathespin K* (b), *Acp5* (c), *DC-stamp* (d), and *Atp6v0d2* (e) mRNA expression in BMDMs with siRNA$^+$ plasmid transfection and RANKL treatment for 5 days, as measured by qPCR.

All data in this figure are represented as mean ± SD. *p < 0.05, **p < 0.01, ***p < 0.005, ****p < 0.001. All experiments were performed in triplicates.

See also Table S1 for qPCR primer sequences.

mechanisms and the factors that determine osteoclastogenesis are not fully understood. It is also unknown if the critical pathways and factors involved in bone homeostasis are regulated by post-translational SUMO modifications. In this study, we report the previously undescribed role of the SUMO2/3 modification and SUMO protease SENP3 in osteoclast differentiation from BMDMs. We observed that SENP3 deficiency dramatically promoted osteoclastogenesis and osteoporosis. De-SUMOylation of IRF8 by SENP3 alleviated osteoclast differentiation under basal and also under the context of estrogen depletion. Our work shows the importance of protein SUMO modification in the process of osteoclastogenesis.

The critical role of SENP3 in osteoclatogenesis suggests that the regulation of SENP3 levels may control the rate of BMDM differentiation into osteoclasts by balancing SUMOylation and de-SUMOylation. Our data showed that during the induction of osteoclast differentiation, SENP3 mRNA levels dramatically decreased. Transcriptional changes in the SENP3 levels might be a quick response to the RANKL signal. However, the protein level of SENP3 during osteoclast differentiation did not decrease as dramatically as the mRNA level. In our previous study, the SENP3 protein accumulated under oxidative stress by attenuating chromatin immunoprecipitation (CHIP)-mediated degradation (Yan et al., 2010); thus, the increased reactive oxygen species (ROS) level during osteoclast differentiation (Li et al., 2014) may stabilize the SENP3 protein. We speculate that this might be the strategy to prevent abrupt osteoclast differentiation. Combining both transcription and protein alteration, the SENP3 protein level was gradually downregulated during osteoclastogenesis. In the rescue experiment, overexpressing SENP3 delayed osteoclast differentiation. Maintaining SENP3 stability and expression could be the potential therapeutic strategy to prevent and treat for bone-resorption-related osteoporosis.

In addition to SENP3, the other SENP family member SENP5 was also downregulated during osteoclast differentiation (Figure 1Cb), suggesting that SENP5 may be involved in the process as well. Correspondingly, we noticed an increased level of global SUMO2/3 conjugation, further indicating that the reduced SENP expression levels resulted in decreased de-SUMOylation during osteoclast differentiation. How the expression and stability of SENPs are regulated upon receiving osteoclast differentiation signals need to be further studied.

For the downstream pathways among the series of SUMO2/3 conjugated proteins, we found and verified that IRF8 was the critical factor negatively regulating osteoclastogenesis. Mutation at the IRF8 SUMO2/3 modification site K310 completely blocked RANKL-induced osteoclast differentiation. Thus, our data demonstrate that IRF8 requires SUMOylation to promote osteoclast differentiation. Because IRF8 was reported to bind to the promoter of NFATc1, additional mechanistic studies are needed to evaluate how SUMOylation affects the binding capacity of IRF8 on the promoter of NFATc1. Our findings underscored the importance of post-translational modifications during bone metabolism and development. The underlying mechanisms of how IRF8 SUMO modification affect osteoclastogenesis during physiological and pathological conditions will aid in the development of novel strategies for the treatment of osteoporosis.

STAR★METHODS

Detailed methods are provided in the online version of this paper and include the following:

- KEY RESOURCES TABLE
- LEAD CONTACT AND MATERIALS AVAILABILITY
- EXPERIMENTAL MODEL AND SUBJECT DETAILS
  - Animals
  - Ovariectomy (OVX) mouse model
  - Bone marrow-derived monocytes (BMDMs) isolation and culture
  - Bone marrow-derived mesenchymal stromal cells (BM-MSCs) isolation and culture
- METHOD DETAILS
  - Skeletal phenotyping
  - Osteoclast differentiation and TRAP staining
  - *In vitro* bone resorption assay
  - Alkaline phosphatase (ALP)/alizarin red staining
  - SiRNA, plasmid, mutagenesis, and transfection
  - Quantitative RT-PCR (qPCR)
  - ELISA
  - Immunoblotting (IB)
  - Tissue histology and Histomorphometry
  - Co-immunoprecipitation (co-IP)
  - Flag immunoprecipitation assay (co-IP with flag M2 beads)
  - Ni-NTA pull down assay
- QUANTIFICATION AND STATISTICAL ANALYSIS
- DATA AND CODE AVAILABILITY

SUPPLEMENTAL INFORMATION

Supplemental Information can be found online at https://doi.org/10.1016/j.celrep.2020.01.036.

ACKNOWLEDGMENTS

We thank Weiguo Zou (Shanghai Institute of Biochemistry and Cell Biology, Chinese Academy of Sciences, University of Chinese Academy of Sciences) for skeletal analysis, Ling Qin (University of Pennsylvania) and Yanqiong Zou (Shanghai Jiao Tong University School of Medicine) for tissue histology analysis, and Yang Chen (Shanghai Jiao Tong University School of Medicine) for image analysis. J. Yang was supported by grants from the National Natural Science Foundation of China (31771522) and Shanghai Municipal Science and Technology Commission (16ZR1418400). X.S. was supported by Foundation of Shanghai Oriental Scholar (TP2018045). Q.W. was supported by grants from the National Natural Science Foundation of China (81272002 and 71432007).

AUTHOR CONTRIBUTIONS

Y.Z., X.S., and Q.W. designed and performed the experiments and wrote the manuscript. K.Y., J. Yang, Y.L., L.D., and G.D. assisted with experiments. L.D. and J. Yi analyzed skeletal phenotyping and tissue histology.

DECLARATION OF INTERESTS

The authors declare no competing interests.

Received: July 8, 2019
Revised: November 19, 2019
Accepted: January 9, 2020
Published: February 11, 2020

REFERENCES

Bae, S., Lee, M.J., Mun, S.H., Giannopoulou, E.G., Yong-Gonzalez, V., Cross, J.R., Murata, K., Giguère, V., van der Meulen, M., and Park-Min, K.H. (2017). MYC-dependent oxidative metabolism regulates osteoclastogenesis via nuclear receptor ERRα. J. Clin. Invest. *127*, 2555–2568.

Black, D.M., and Rosen, C.J. (2016). Clinical Practice. Postmenopausal Osteoporosis. N. Engl. J. Med. *374*, 254–262.

Black, D.M., Cummings, S.R., Karpf, D.B., Cauley, J.A., Thompson, D.E., Nevitt, M.C., Bauer, D.C., Genant, H.K., Haskell, W.L., Marcus, R., et al.; Fracture Intervention Trial Research Group (1996). Randomised trial of effect of alendronate on risk of fracture in women with existing vertebral fractures. Lancet *348*, 1535–1541.

Chang, T.H., Xu, S., Tailor, P., Kanno, T., and Ozato, K. (2012). The small ubiquitin-like modifier-deconjugating enzyme sentrin-specific peptidase 1 switches IFN regulatory factor 8 from a repressor to an activator during macrophage activation. J. Immunol. *189*, 3548–3556.

Chen, W., Zhu, G., Jules, J., Nguyen, D., and Li, Y.P. (2018). Monocyte-Specific Knockout of C/ebpalpha Results in Osteopetrosis Phenotype, Blocks Bone Loss in Ovariectomized Mice, and Reveals an Important Function of C/ebpalpha in Osteoclast Differentiation and Function. J. Bone Miner. Res. *33*, 691–703.

Cummings, S.R., San Martin, J., McClung, M.R., Siris, E.S., Eastell, R., Reid, I.R., Delmas, P., Zoog, H.B., Austin, M., Wang, A., et al.; FREEDOM Trial (2009). Denosumab for prevention of fractures in postmenopausal women with osteoporosis. N. Engl. J. Med. *361*, 756–765.

Dempster, D.W., Compston, J.E., Drezner, M.K., Glorieux, F.H., Kanis, J.A., Malluche, H., Meunier, P.J., Ott, S.M., Recker, R.R., and Parfitt, A.M. (2013). Standardized nomenclature, symbols, and units for bone histomorphometry: a 2012 update of the report of the ASBMR Histomorphometry Nomenclature Committee. J. Bone Miner. Res. *28*, 2–17.

Di Iorgi, N., Rosol, M., Mittelman, S.D., and Gilsanz, V. (2008). Reciprocal relation between marrow adiposity and the amount of bone in the axial and appendicular skeleton of young adults. J. Clin. Endocrinol. Metab. *93*, 2281–2286.

Ettinger, B., Black, D.M., Mitlak, B.H., Knickerbocker, R.K., Nickelsen, T., Genant, H.K., Christiansen, C., Delmas, P.D., Zanchetta, J.R., Stakkestad, J., et al.; Multiple Outcomes of Raloxifene Evaluation (MORE) Investigators (1999). Reduction of vertebral fracture risk in postmenopausal women with osteoporosis treated with raloxifene: results from a 3-year randomized clinical trial. JAMA *282*, 637–645.

Farr, J.N., Xu, M., Weivoda, M.M., Monroe, D.G., Fraser, D.G., Onken, J.L., Negley, B.A., Sfeir, J.G., Ogrodnik, M.B., Hachfeld, C.M., et al. (2017). Targeting cellular senescence prevents age-related bone loss in mice. Nat. Med. *23*, 1072–1079.

Ghisletti, S., Huang, W., Ogawa, S., Pascual, G., Lin, M.E., Willson, T.M., Rosenfeld, M.G., and Glass, C.K. (2007). Parallel SUMOylation-dependent pathways mediate gene- and signal-specific transrepression by LXRs and PPARgamma. Mol. Cell *25*, 57–70.

Han, Y., Huang, C., Sun, X., Xiang, B., Wang, M., Yeh, E.T., Chen, Y., Li, H., Shi, G., Cang, H., et al. (2010). SENP3-mediated de-conjugation of SUMO2/3 from promyelocytic leukemia is correlated with accelerated cell proliferation under mild oxidative stress. J. Biol. Chem. *285*, 12906–12915.

Harris, S.T., Watts, N.B., Genant, H.K., McKeever, C.D., Hangartner, T., Keller, M., Chesnut, C.H., 3rd, Brown, J., Eriksen, E.F., Hoseyni, M.S., et al.; Vertebral Efficacy With Risedronate Therapy (VERT) Study Group (1999). Effects of risedronate treatment on vertebral and nonvertebral fractures in women with postmenopausal osteoporosis: a randomized controlled trial. JAMA *282*, 1344–1352.

Hendriks, I.A., Lyon, D., Su, D., Skotte, N.H., Daniel, J.A., Jensen, L.J., and Nielsen, M.L. (2018). Site-specific characterization of endogenous SUMOylation across species and organs. Nat. Commun. *9*, 2456.

Huang, C., Han, Y., Wang, Y., Sun, X., Yan, S., Yeh, E.T., Chen, Y., Cang, H., Li, H., Shi, G., et al. (2009). SENP3 is responsible for HIF-1 transactivation under mild oxidative stress via p300 de-SUMOylation. EMBO J. *28*, 2748–2762.

Huang, W., Ghisletti, S., Saijo, K., Gandhi, M., Aouadi, M., Tesz, G.J., Zhang, D.X., Yao, J., Czech, M.P., Goode, B.L., et al. (2011). Coronin 2A mediates actin-dependent de-repression of inflammatory response genes. Nature *470*, 414–418.

Kanis, J.A., McCloskey, E.V., Johansson, H., Cooper, C., Rizzoli, R., and Reginster, J.Y. (2013). European guidance for the diagnosis and management of osteoporosis in postmenopausal women. Osteoporosis Int. *24*, 23–57.

Kim, K., Kim, J.H., Lee, J., Jin, H.M., Lee, S.H., Fisher, D.E., Kook, H., Kim, K.K., Choi, Y., and Kim, N. (2005a). Nuclear factor of activated T cells c1 induces osteoclast-associated receptor gene expression during tumor necrosis factor-related activation-induced cytokine-mediated osteoclastogenesis. J. Biol. Chem. *280*, 35209–35216.

Kim, Y., Sato, K., Asagiri, M., Morita, I., Soma, K., and Takayanagi, H. (2005b). Contribution of nuclear factor of activated T cells c1 to the transcriptional control of immunoreceptor osteoclast-associated receptor but not triggering receptor expressed by myeloid cells-2 during osteoclastogenesis. J. Biol. Chem. *280*, 32905–32913.

Kim, K., Kim, J.H., Lee, J., Jin, H.M., Kook, H., Kim, K.K., Lee, S.Y., and Kim, N. (2007a). MafB negatively regulates RANKL-mediated osteoclast differentiation. Blood *109*, 3253–3259.

Kim, K., Lee, J., Kim, J.H., Jin, H.M., Zhou, B., Lee, S.Y., and Kim, N. (2007b). Protein inhibitor of activated STAT 3 modulates osteoclastogenesis by down-regulation of NFATc1 and osteoclast-associated receptor. J .Immunol. *178*, 5588–5594.

Kim, J.H., Youn, B.U., Kim, K., Moon, J.B., Lee, J., Nam, K.I., Park, Y.W., O'Leary, D.D., Kim, K.K., and Kim, N. (2014). Lhx2 regulates bone remodeling in mice by modulating RANKL signaling in osteoclasts. Cell Death Differ. *21*, 1613–1621.

Lao, Y., Yang, K., Wang, Z., Sun, X., Zou, Q., Yu, X., Cheng, J., Tong, X., Yeh, E.T.H., Yang, J., and Yi, J. (2018). DeSUMOylation of MKK7 kinase by the SUMO2/3 protease SENP3 potentiates lipopolysaccharide-induced inflammatory signaling in macrophages. J. Biol. Chem. *293*, 3965–3980.

Lee, J., Kim, K., Kim, J.H., Jin, H.M., Choi, H.K., Lee, S.H., Kook, H., Kim, K.K., Yokota, Y., Lee, S.Y., et al. (2006). Id helix-loop-helix proteins negatively regulate TRANCE-mediated osteoclast differentiation. Blood *107*, 2686–2693.

Li, D.Z., Zhang, Q.X., Dong, X.X., Li, H.D., and Ma, X. (2014). Treatment with hydrogen molecules prevents RANKL-induced osteoclast differentiation associated with inhibition of ROS formation and inactivation of MAPK, AKT and NF-kappa B pathways in murine RAW264.7 cells. J. Bone Miner. Metab. *32*, 494–504.

Li, J., Lu, D., Dou, H., Liu, H., Weaver, K., Wang, W., Li, J., Yeh, E.T.H., Williams, B.O., Zheng, L., and Yang, T. (2018). Desumoylase SENP6 maintains osteochondroprogenitor homeostasis by suppressing the p53 pathway. Nat. Commun. *9*, 143.

Liu, K., Guo, C., Lao, Y., Yang, J., Chen, F., Zhao, Y., Yang, Y., Yang, J., and Yi, J. (2019). A fine-tuning mechanism underlying self-control for autophagy: deSUMOylation of BECN1 by SENP3. Autophagy *2*, 1–16.

Matsumoto, M., Kogawa, M., Wada, S., Takayanagi, H., Tsujimoto, M., Katayama, S., Hisatake, K., and Nogi, Y. (2004). Essential role of p38 mitogen-activated protein kinase in cathepsin K gene expression during osteoclastogenesis through association of NFATc1 and PU.1. J. Biol. Chem. *279*, 45969–45979.

Matsumoto, T., Hagino, H., Shiraki, M., Fukunaga, M., Nakano, T., Takaoka, K., Morii, H., Ohashi, Y., and Nakamura, T. (2009). Effect of daily oral minodronate on vertebral fractures in Japanese postmenopausal women with established osteoporosis: a randomized placebo-controlled double-blind study. Osteoporosis Int. *20*, 1429–1437.

Miyauchi, Y., Ninomiya, K., Miyamoto, H., Sakamoto, A., Iwasaki, R., Hoshi, H., Miyamoto, K., Hao, W., Yoshida, S., Morioka, H., et al. (2010). The Blimp1-Bcl6 axis is critical to regulate osteoclast differentiation and bone homeostasis. J. Exp. Med. *207*, 751–762.

Nayak, A., Viale-Bouroncle, S., Morsczeck, C., and Muller, S. (2014). The SUMO-specific isopeptidase SENP3 regulates MLL1/MLL2 methyltransferase complexes and controls osteogenic differentiation. Mol. Cell *55*, 47–58.

Park, K.R., Kim, E.C., Hong, J.T., and Yun, H.M. (2018). Dysregulation of 5-hydroxytryptamine 6 receptor accelerates maturation of bone-resorbing osteoclasts and induces bone loss. Theranostics *8*, 3087–3098.

Pascual, G., Fong, A.L., Ogawa, S., Gamliel, A., Li, A.C., Perissi, V., Rose, D.W., Willson, T.M., Rosenfeld, M.G., and Glass, C.K. (2005). A SUMOylation-dependent pathway mediates transrepression of inflammatory response genes by PPAR-gamma. Nature *437*, 759–763.

Schuit, S.C., van der Klift, M., Weel, A.E., de Laet, C.E., Burger, H., Seeman, E., Hofman, A., Uitterlinden, A.G., van Leeuwen, J.P., and Pols, H.A. (2004). Fracture incidence and association with bone mineral density in elderly men and women: the Rotterdam Study. Bone *34*, 195–202.

Stegen, S., Stockmans, I., Moermans, K., Thienpont, B., Maxwell, P.H., Carmeliet, P., and Carmeliet, G. (2018). Osteocytic oxygen sensing controls bone mass through epigenetic regulation of sclerostin. Nat. Commun. *9*, 2557.

Suire, C., Brouard, N., Hirschi, K., and Simmons, P.J. (2012). Isolation of the stromal-vascular fraction of mouse bone marrow markedly enhances the yield of clonogenic stromal progenitors. Blood *119*, e86–e95.

Takayanagi, H. (2007). Osteoimmunology: shared mechanisms and crosstalk between the immune and bone systems. Nat. Rev. Immunol. *7*, 292–304.

Takayanagi, H., Kim, S., Koga, T., Nishina, H., Isshiki, M., Yoshida, H., Saiura, A., Isobe, M., Yokochi, T., Inoue, J., et al. (2002). Induction and activation of the transcription factor NFATc1 (NFAT2) integrate RANKL signaling in terminal differentiation of osteoclasts. Dev. Cell *3*, 889–901.

Teitelbaum, S.L. (2000). Bone resorption by osteoclasts. Science *289*, 1504–1508.

Wang, Y., and Dasso, M. (2009). SUMOylation and deSUMOylation at a glance. J. Cell Sci. *122*, 4249–4252.

Wu, D.J., Gu, R., Sarin, R., Zavodovskaya, R., Chen, C.P., Christiansen, B.A., Zarbalis, K.S., and Adamopoulos, I.E. (2016). Autophagy-linked FYVE containing protein WDFY3 interacts with TRAF6 and modulates RANKL-induced osteoclastogenesis. J. Autoimmun. *73*, 73–84.

Yan, S., Sun, X., Xiang, B., Cang, H., Kang, X., Chen, Y., Li, H., Shi, G., Yeh, E.T., Wang, B., et al. (2010). Redox regulation of the stability of the SUMO protease SENP3 via interactions with CHIP and Hsp90. EMBO J. *29*, 3773–3786.

Zhao, B., Takami, M., Yamada, A., Wang, X., Koga, T., Hu, X., Tamura, T., Ozato, K., Choi, Y., Ivashkiv, L.B., et al. (2009). Interferon regulatory factor-8 regulates bone metabolism by suppressing osteoclastogenesis. Nat. Med. *15*, 1066–1071.

Zhou, Z., Wang, M., Li, J., Xiao, M., Chin, Y.E., Cheng, J., Yeh, E.T., Yang, J., and Yi, J. (2016). SUMOylation and SENP3 regulate STAT3 activation in head and neck cancer. Oncogene *35*, 5826–5838.

STAR★METHODS

KEY RESOURCES TABLE

REAGENT or RESOURCE	SOURCE	IDENTIFIER
Antibodies		
Rabbit polyclonal anti-SUMO1	Cell Signaling Technology	Cat#4940; RRID:AB_2302825
Rabbit polyclonal anti-SUMO2/3	Cell Signaling Technology	Cat#4971
Rabbit polyclonal anti-SENP3	Cell Signaling Technology	Cat#5591; RRID:AB_10694546
Rabbit polyclonal anti-IRF8	Cell Signaling Technology	Cat#5628; RRID:AB_10828231
Rabbit polyclonal anti-NFATc1	Cell Signaling Technology	Cat#8032; RRID:AB_10829466
Mouse monoclonal anti-RGS-His	QIAGEN	Cat#34610
Mouse monoclonal anti-HA	Covance	Cat#MMS-101P; RRID:AB_2314672
Mouse monoclonal anti-Flag	Sigma-Aldrich	Cat#F3165; RRID:AB_259529
Mouse monoclonal anti-β-actin	Sigma-Aldrich	Cat#A5441; RRID:AB_476744
Mouse monoclonal anti-Cathespin K	Santa Cruz	Cat#48353
Rabbit polyclonal anti-c-fos	Cell Signaling Technology	Cat#2250; RRID:AB_2247211
Chemicals, Peptides, and Recombinant Proteins		
Recombinant Murine M-CSF	Peprotech	Cat#315-02
Recombinant Mouse TRANCE/ TNFSF11/RANKL	R&D systems	Cat#462-TEC-010
type I collagenase	Worthington	Cat#LS004194
Dispase	Roche Diagnostic	Cat#10269638001
DNase I	Sigma-Aldrich	Cat#9003-98-9
Attractene Transfenction Reagent	QIAGEN	Cat#301007
β-sodium glycerophosphate	Sigma-Aldrich	Cat#50020
Alizarin red	Sigma-Aldrich	Cat#A5533
Calcein	Sigma-Aldrich	Cat#C0875
Ni2+-NTA-agarose resin	QIAGEN	Cat#30210
protein A/G-agarose	Pierce	Cat#20421
Anti-Flag M2 Affinity Gel	Sigma-Aldrich	Cat#A2220; RRID:AB_10063035
Ascorbic acid	Sigma-Aldrich	Ca#A5960
Critical Commercial Assays		
TRAP staining kit	Sigma-Aldrich	Cat#387A
Mouse CTX I (Cross Linked C-telopeptide of Type I Collagen) ELISA Kit	Elabscience	Cat#E-EL-M0366c
Mouse PINP (Procollagen I N-Terminal Propedtide) ELISA Kit	Elabscience	Cat#E-EL-M0233c
Experimental Models: Cell Lines		
HEK293T	ATCC	Cat#CRL-3216; RRID:CVCL_0063
Experimental Models: Organisms/Strains		
Mouse: C57/B6 SENP3 fl/fl; Lyz2-cre	Lao et al., 2018	N/A
Mouse: C57/B6 SENP3 flox mice	Model Animal Research Center of Nanjing University (Nanjing, China)	N/A
Oligonucleotides		
siRNA targeting sequence: SENP3: GGGCUGGAAAGGUUACUUCAAdTdT	Han et al., 2010	N/A
Scramble siRNA	Han et al., 2010	N/A
Primers for qPCR, see Table S1	This paper	N/A

(*Continued on next page*)

Continued

REAGENT or RESOURCE	SOURCE	IDENTIFIER
Recombinant DNA		
Plasmid: Flag-SENP3	Lao et al., 2018	N/A
Plasmid: Flag-SENP3 C532A mutant	Lao et al., 2018	N/A
Plasmid: RH-SENP3	Yan et al., 2010	N/A
Plasmid: RH-SUMO3	Yan et al., 2010	N/A
Plasmid: pcDNA3.1	Yan et al., 2010	N/A
Plasmid: UBC9	Yan et al., 2010	N/A
Plasmid: p3 × FLAG-CMV-10	Shanghai TranSheepBio Biological Technology Co. Ltd	N/A
Plasmid: Flag-IRF8	This paper	N/A
Plasmid: Flag-IRF8 K310R mutant	This paper	N/A
Plasmid: HA-SENP3	This paper	N/A
Plasmid: HA-SENP3 C532A mutant	This paper	N/A
Software and Algorithms		
Graphpad Prism 7	Graphpad	https://www.graphpad.com/
SPSS statistics software 19.0	IBM SPSS	https://www.ibm.com/analytics/spss-statistics-software
ImageJ Software	ImageJ	https://imagej.nih.gov/ij

LEAD CONTACT AND MATERIALS AVAILABILITY

Plasmids generated in this study are available on request. Further information and reagents should be directed to and will be fulfilled by Lead Contact, Qiugen Wang (wangqiugen@126.com). This study did not generate new unique reagents.

EXPERIMENTAL MODEL AND SUBJECT DETAILS

Animals

C57BL/6 wild-type mice were purchased from the Shanghai SLAC Laboratory Animal Co. Ltd. Male and female mice at eight- to twelve-week old were used for experiments as noted in figures and legends. All mice were maintained under specific pathogen free (SPF) condition in a barrier-sustained facility and provided with sterile food and water. *Senp3*$^{flox/flox}$*; Lyz2-Cre* mice were generated as described previously (Lao et al., 2018). Animal experiments were carried out in accordance with the regulations in the Guide for the Care and Use of Laboratory Animals issued by the Ministry of Science and Technology of the People's Republic of China. The protocol was approved by the Institutional Animal Care & Use Committee of Shanghai Jiao Tong University School of Medicine (Permit Number: A-2016-023). All surgery was performed under chloral hydrate anesthesia, and every effort was made to minimize suffering.

Ovariectomy (OVX) mouse model

Ovariectomy (OVX) was performed in 12-week old female mice. After anaesthetization (3.5% Chloral hydrate, 10 mL/kg body weight). The left and right ovary were exposed and removed; in the sham-operated (sham) animals, the ovaries were exposed but left intact. Four weeks after OVX, mice were sacrificed, blood was collected and long bones were dissected for histology and microCT analysis.

Bone marrow-derived monocytes (BMDMs) isolation and culture

Bone marrow-derived monocytes (BMDMs) were isolated from *Senp3*$^{flox/flox}$ (referred to as "WT") or *Senp3*$^{flox/flox}$*; Lyz2-Cre* mice as previous described (Lao et al., 2018). Briefly, mice were dissected under chloral hydrate anesthesia and sterilized with 75% ethanol. The bones were flushed using a syringe filled with α-MEM (GIBCO) to extrude bone marrow. Cell suspensions were filtered through a 100 μm cell strainer. After 24hr, the bone marrow cells were attached and induced to differentiate in α-MEM supplemented with 10% fetal bovine serum (GIBCO), 1% penicillin/streptomycin (Invitrogen), and 50 ng/ml murine macrophage colony-stimulating factor (M-CSF) (Peprotech). BMDMs were collected at day 3 after M-CSF stimuli and identified by flow cytometry with FITC-F4/80 (eBioscience) and APC-CD11b (BD) antibodies (data not shown).

Bone marrow-derived mesenchymal stromal cells (BM-MSCs) isolation and culture

Enzymatic digestion of bone marrow cells and CFU-F cultures were performed as described previously (Suire et al., 2012). Briefly, intact marrow plugs were flushed from the long bones and subjected to two rounds of enzymatic digestion at 37°C for 15 min each.

The digestion buffer contained 3 mg/ml type I collagenase (Worthington), 4 mg/ml dispase (Roche Diagnostic) and 1 U/ml DNase I (Sigma) in HBSS with calcium and magnesium. The cells were resuspended in staining medium (HBSS+2%FBS) with 2 mM EDTA to stop the digestion. Freshly dissociated single cell suspensions were plated at in 10 cm plates (5×10^6 cells/dish) with α-MEM, 20% FBS, 10 mM ROCK inhibitor (Y-27632, TOCRIS), and 1% penicillin/streptomycin. The culture medium was changed on the second day after plating to wash out macrophages, then changed every 3-4 days.

METHOD DETAILS

Skeletal phenotyping

MicroCT and quantitative analysis of distal femoral metaphysis was performed by Shanghai Saixin Biological Technology Co. Ltd. 3D analysis was used to calculate morphometric parameters at distal femoral metaphysis (200 slices). Trabecular bone mass and microarchitecture were defined including trabecular bone volume/tissue volume ratio (BV/TV), bone surface/ bone volume ratio (BS/BV), trabecular number (Tb.N), trabecular thickness (Tb.Th), trabecular separation (Tb.Sp), while cortical bone mass and microarchitecture were defined including cortical bone volume/tissue volume ratio (Ct.BV/TV), cortical bone surface/ bone volume ratio (Ct.BS/BV), cortical thickness (Ct.Th) and cortical bone mass density (Ct.BMD). All imaging were performed in a blinded fashion as described (Farr et al., 2017).

Osteoclast differentiation and TRAP staining

Osteoclast differentiation induction was performed as described (Zhao et al., 2009). Briefly, harvested BMDMs was cultured with α-MEM supplemented with 10% fetal bovine serum, 50 ng/ml murine M-CSF (Peprotech) and 100 ng/ml murine RANKL (R&D). The medium was replaced every other day. Pre-osteoclasts and mature osteoclasts were evaluated using TRAP staining kit (Sigma) at different time points. The number of TRAP positive BMDMs in one field of vision, osteoclast size of TRAP positive BMDMs and the number of TRAP positive BMDMs with > 3 nuclei were measured as described (Park et al., 2018; Wu et al., 2016).

In vitro bone resorption assay

Bone resorption activity was assessed as described previously (Chen et al., 2018). Briefly, BMDMs was collected and co-cultured with bovine cortical bone slices in 48-well plates. Cells were then treated with RANKL/M-CSF for 5-6 days. 0.25 M ammonium hydroxide and mechanical agitation were used to remove cells adhering to the bone slices. Bone resorption pits were analyzed by 1% toluidine blue staining. Quantification was achieved by measuring the percentage of the areas resorbed in three random resorption sites using ImageJ software.

Alkaline phosphatase (ALP)/alizarin red staining

Osteogenic differentiation was assessed by ALP and alizarin red staining. BM-MSCs were isolated as above description. On the second day, the medium was replaced with osteogenic α-MEM medium containing 10%FBS, 10mM β-sodium glycerophosphate (Sigma), 50 μg/mL ascorbic acid (Sigma). The culture medium was replaced every other day. 7-14 days later, the colonies that contained osteoblasts were assessed by ALP staining (Cell Biolabs) and alizarin red staining (Sigma) according to manufacturer's protocol, respectively.

SiRNA, plasmid, mutagenesis, and transfection

The siRNA specific for SENP3 and scramble siRNA oligonucleotides were synthesized and used as previously described (Han et al., 2010). The plasmids of RH-SENP3, RH-SUMO3, UBC9, pcDNA3.1 were constructed and used as previously described (Yan et al., 2010). The plasmid Flag-IRF8, Flag-IRF8 K310R mutant, HA-SENP3, HA-SENP3 C532A mutant and p3 × FLAG-CMV-10 were generated by Shanghai TranSheepBio Biological Technology Co. Ltd.

Attractene Transfenction Reagent (ATR, QIAGEN, Germany) was used for transfection reagent as described (Lao et al., 2018). Briefly, the day before transfection, an appropriate amount of cells were seeded into the plate with the density 60% to 80% during transfection. The siRNA-ATR/plasmid-ATR mixture were added it to the plate, gently shaken and mixed; the plate was placed in a 37°C incubator overnight. Culture medium was changed after 12 hours and then incubated for another 24-48 hours.

Quantitative RT-PCR (qPCR)

This method was as previously described (Zhou et al., 2016). Total RNA was isolated from cells using trizol reagent (Invitrogen), and cDNA was synthesis using high-capacity cDNA reverse transcription kit (Invitrogen). Quantitative real-time PCR was conducted using SYBR Green (Roche) on the Roche LightCycler 480 system. See Table S1 for primers used.

ELISA

Blood was collected from mice and clotted for 2 hours at room temperature before centrifuge for 30 min at 2000 g, and serum was harvested and stored at −80°C for subsequent assays as described (Lao et al., 2018). Type 1 collagen amino-terminal propeptide (P1NP) and type 1 collagen C breakdown products (CTX-1) concentrations in the serum were examined using mouse ELISA kits (Elabscience) according to the manufacturer's instructions.

Immunoblotting (IB)

IB was performed using the routine methods as described (Huang et al., 2009). The following antibodies were used: SUMO1 (Cell Signaling, 4940), SUMO2/3 (Cell Signaling, 4971), SENP3 (Cell Signaling, 5591), IRF8 (Cell Signaling, 5628), NFATc1 (Cell Signaling, 8032), RH (QIAGEN, 34610), HA (Covance, MMS-101P), Flag (Sigma, F3165) and β-actin (Sigma, A5441), c-*fos* (Cell Signaling, 2250), Cathespin K (Santa Cruz, 48353).

Tissue histology and Histomorphometry

For histology, bones were fixed overnight at 4°C in 4% paraformaldehyde, decalcified for 2 weeks in 10% (wt/wt) EDTA (pH 7.4), and embedded in paraffin. Undecalcified bones were fixed overnight at 4°C in Burckhart's solution and embedded in methylmetacrylate (MMA). Osteoblast number and surface were quantified on H&E-stained sections, and osteoblast surface were expressed relatively to the total bone surface as Ob.S/BS. Osteoclast parameters were measured on TRAP stained sections. Paraffin sections were stained in TRAP working buffer (Sigma) for 1h at 37°C and then in hematoxylin (Prosan) for 1 min. Osteoclast surface were analyzed relatively to the total bone surface as Oc.S/BS (Stegen et al., 2018).

To analyze dynamic bone parameters, 16mg/kg body weight calcein (Sigma-Aldrich) was administered via intraperitoneal injection 7 days and 3 day prior to sacrifice(Stegen et al., 2018; Zhao et al., 2009). The mineralizing surface (MS), mineral apposition rate (MAR) and bone formation rate/bone surface ratio (BFR/BS) were quantified on unstained MMA-sections. MAR was quantified as the mean distance between all double fluorochrome labels, divided by the number of days between calcein injections. BFR/BS was calculated as (MS = (dLS + sLS/2)/BS)*MAR, where dLS and sLS represent the bone surface covered by double (d) and single (s) calcein labels. Measurements were done on three sections, each at least 40 μm apart and data were presented according to the guidelines of the American Society for Bone and Mineral Research standardized histomorphometry nomenclature (Dempster et al., 2013).

Co-immunoprecipitation (co-IP)

The co-IP was performed using methods described previously (Huang et al., 2009). Briefly, cells were lysed in RIPA buffer (Thermo Fisher Scientific) for 30 min at 4°C, and then centrifuged at 13000 g at 4°C for 30 min. The lysates were incubated with protein A/G-agarose (Pierce) for 2 hours at 4°C for preclearing. Specific antibodies were incubated overnight at 4°C followed by protein-A/G agarose beads incubation at 4°C for 4 hours next day. The beads were then washed 6 times, mixed with loading buffer and examined by IB.

Flag immunoprecipitation assay (co-IP with flag M2 beads)

The routine flag immunoprecipitation assay was carried out using methods described previously (Liu et al., 2019). Briefly, transfected cells were lysed in a lysis buffer (50 mM Tris-HCl, pH 7.4, with 150 mM NaCl, 1 mM EDTA and 1%Triton X-100) for 30 min at 4°C, then centrifuged at 13000 g at 4°C for 30 min. Anti-Flag M2 Affinity Gel (Sigma Aldrich) was added to the cell lysates and incubated overnight at 4°C. After six times washing, samples were eluted in the elution buffer and examined by IB.

Ni-NTA pull down assay

Ni-nitrilotriacetic acid resin (NTA) pull down analysis was performed as previously described (Huang et al., 2009). Briefly, the cells were transfected with RH tagged plasmid. Transfected cells were lysed in a specific lysis buffer according to the manufacturers' protocols. Ni^{2+}-NTA-agarose resin (QIAGEN) was then added to the cell lysates and incubated with gentle agitation at 4°C overnight. The resin was successively washed at room temperature with wash buffers. After washing, RH-tagged proteins were eluted in elution buffer and then subjected to IB.

QUANTIFICATION AND STATISTICAL ANALYSIS

Statistical significance was calculated by Student's t test for two-sample comparisons and one-way ANOVA was used for multiple comparisons in software SPSS 19.0. And Turkey's test was used to find significant differences in ANOVA. Statistical significance was analyzed on data from at least three independent experiments. *$p < 0.05$, **$p < 0.01$, ***$p < 0.005$ and ****$p < 0.0001$ were defined as significant. All data are presented as mean ± SD unless otherwise specified.

DATA AND CODE AVAILABILITY

Raw data and images have not been deposited in a public repository because the manuscript is in preparation, but are available from the corresponding author on request. This study did not generate any dataset or code.